Interpreting the $^{13}C/^{12}C$ ratio of carbon dioxide in an urban airshed in the Yangtze River Delta, China

Jiaping Xu[1], Xuhui Lee[1,2*], Wei Xiao[1], Chang Cao[1], Shoudong Liu[1], Xuefa Wen[3], Jingzheng Xu[1], Zhen Zhang[1], Jiayu Zhao[1]

[1]Yale-NUIST Center on Atmospheric Environment, Nanjing University of Information Science & Technology, Nanjing, China

[2]School of Forestry and Environmental Studies, Yale University, New Haven, Connecticut, USA

[3]Key Laboratory of Ecosystem Network Observation and Modeling, Institute of Geographic Sciences and Natural Resources Research, Chinese Academy of Sciences, Beijing, China

* Corresponding author
Dr. Xuhui Lee
Sara Shallenberger Brown Professor
School of Forestry and Environmental Studies, Yale University,
21 Sachem Street, New Haven, Connecticut 06510, USA
Phone: (203)432-6271; Fax: (203)432-5023
E-mail: xuhui.lee@yale.edu

Abstract: Observations of atmospheric CO_2 mole fraction and the $^{13}C/^{12}C$ ratio (expressed as $\delta^{13}C$) in urban airsheds provide constraints on the roles of anthropogenic and natural sources and sinks in local and regional carbon cycles. In this study, we report observations of these quantities in Nanjing at hourly intervals from March 2013 to August 2015 using a laser-based optical instrument. Nanjing is the second largest city located in the highly industrialized Yangtze River Delta (YRD), Eastern China. The mean CO_2 mole fraction and $\delta^{13}C$ were (439.7 ± 7.5) μmol mol^{-1} and (-8.48 ± 0.56) ‰ over this observational period. The peak monthly mean $\delta^{13}C$ (-7.44 ‰, July 2013) was 0.74 ‰ higher than that observed at Mount Waliguan, a WMO baseline site on the Tibetan Plateau and upwind of the YRD region. The highly ^{13}C-enriched signal was partly attributed to the influence of cement production in the region. By applying the Miller-Tans method to nighttime and daytime observations to represent signals from the city of Nanjing and the YRD, respectively, we showed that the $^{13}C/^{12}C$ ratio of CO_2 sources in the Nanjing Municipality was (0.21 ± 0.53) ‰ lower than that in the YRD. Flux partitioning calculations revealed that natural ecosystems in the YRD were a negligibly small source of atmospheric CO_2.

Keywords: urban areas; CO_2 flux; Industrial process; Carbon isotope; In-situ observation

1 Introduction

Atmospheric CO_2 sources and sinks in urban areas consist mainly of plant uptake and release and fossil fuel combustion. These contributors have unique $^{13}C/^{12}C$ ratios. City clusters are human-dominated systems with high carbon emission intensity, contributing over 70% of the total anthropogenic CO_2 to the atmosphere (Satterthwaite 2008). Previous urban isotopic studies emphasize carbon emissions from fossil combustion (Zondervan and Meijer 1996, Pataki et al. 2003, Zimnoch et al. 2004, Affek and Eiler 2006, Newman et al. 2008). Relatively little attention is given to the $\delta^{13}C$ of carbon dioxide released by cement production, which is much higher than that of fossil fuel origin (Andres et al. 1994). Likewise, the CO_2 emitted from burning of minerals in non-energy consumption industrial processes, such as iron and steel production, has higher $\delta^{13}C$ than that of fossil fuel (Table 2, Widory 2006). In China, cement production and industrial processes contribute 13 % of the total anthropogenic CO_2 emission (Mu et al. 2013). Many of these industrial activities occur in or near urban areas. So far, little is known about their roles in the atmospheric carbon stable isotope budget.

One scientific motivation for quantifying the $\delta^{13}C$ of atmospheric CO_2 is that it provides constraints that allow partitioning of the net surface flux into component fluxes (Farquhar and Lloyd 1993, Yakir and Sternberg 2000, Pataki et al. 2003). The ^{13}C-based partitioning method has been used primarily for vegetation ecosystems, such as forests (Lloyd et al. 1996, Lloyd et al. 2001, Ometto, et al. 2006, Zobitz et al. 2008), grasses (Ometto et al. 2002, Pataki et al. 2003), and crops (Leavitt et al. 1995, Griffis et al. 2005). The approach has also been used in a limited number of urban studies (Pataki et al. 2003, Zimnoch et al. 2004, Newman et al.

2008, Jasek et al. 2014). Compared with vegetation ecosystems, urban ecosystems have more complex CO_2 source configurations. We must consider both natural sources (plants and soils) and anthropogenic sources (fossil combustion and non-energy industrial processes) and the fact that the degree of mixing of urban air with the free troposphere and the air outside the urban boundary varies diurnally and seasonally. Anthropogenic emissions are hard to quantify because they depend on multiple factors including city size, population density, fossil mix, and climate.

One of the first measurements of the carbon isotope ratio of CO_2 in an urban atmosphere was made by Friedman and Irsa (1967). Since then, more experiments have been conducted in urban environments (Ehleringer et al. 2002, Koerner and Klopatek 2002, Takahashi et al. 2002, Clark-Thorne and Yapp 2003, Lichtfouse et al. 2003, Widory and Javoy 2003, Zimnoch et al. 2004, Bush et al. 2007, Guha and Ghosh 2010, Wang and Pataki 2012). The analytical technique employed in these studies is mainly based on isotope-ratio mass-spectrometry (IRMS). In recent years, the development of isotope ratio infrared spectroscopy (IRIS) and on-line calibration technology provides a new solution for long-term in-situ observation of the CO_2 mole fraction and $\delta^{13}C$ at high frequencies (1 Hz to 1 hour; Pataki et al. 2006, Griffis. 2013, Gorski et al. 2015). However, application of the IRIS technology in urban monitoring is still limited in terms of cities covered and measurement duration (McManus et al. 2002, Pataki et al. 2006, Wada et al. 2011, Moore and Jacobson (2015). Only a few published studies have presented data that span one full annual cycle (e.g., Pang et al. 2016).

Simultaneous measurement of atmospheric CO_2 concentration and $\delta^{13}C$ is used to determine the overall $^{13}C/^{12}C$ ratio of local surface sources δ_S. The majority of published

86 urban studies to date have deployed the Keeling plot method (Keeling 1958, Keeling 1961)
87 for the determination of δ_S. In this approach, a linear relationship is established between $\delta^{13}C$
88 and the reciprocal of the CO_2 mole fraction from the observed time series, and the intercept
89 of the linear regression is taken as the isotopic ratio of the local CO_2 emissions. The method
90 assumes that the isotopic ratio of the sources is invariant with time. It also assumes that
91 changes in the CO_2 mole fraction and in $\delta^{13}C$ are attributed only to the surface sources and
92 are unaffected by regional carbon sources (Pataki et al. 2003). However, these assumptions
93 do not strictly hold in an urban environment because the intensity of traffic emissions varies
94 strongly through the diel cycle (McDonald et al. 2014), and therefore the composition of the
95 surface source varies, and its $^{13}C/^{12}C$ ratio cannot be assumed constant. In addition, because
96 of strong atmospheric mixing in the daytime convective boundary layer, the background air
97 in the upper troposphere can be easily entrained to the surface layer, mixing the CO_2 that
98 originates from regional sources with that emitted locally in the urban airshed.
99 Miller and Tans (2003) propose that δ_S be determined as the slope of the linear
100 relationship
101 $$\delta_a C_a - \delta_b C_b = \delta_S (C_a - C_b) \quad (1)$$
102 where C_a is CO_2 mole fraction in urban air, C_b is CO_2 mole fraction at a background site, δ_a is
103 the $\delta^{13}C$ value of C_a, and δ_b is the $\delta^{13}C$ value of C_b. All the variables are time dependent.
104 Because this approach takes into account the fact the background atmosphere varies, it may
105 be more suitable than the Keeling method for inferring δ_S from the observations made in the
106 urban area with complex emission sources. The method has been applied to local and
107 regional carbon budget studies in nonurban settings (Miller et al. 2003) and in an urban

environment by Newman et al. (2016). Here we extend the method to continuous measurements in an urban environment.

In this study, we report the results of long-term (30 months) continuous measurement of atmospheric CO_2 mole fraction and $\delta^{13}C$ at a suburban site in Nanjing using an IRIS instrument. Nanjing is the second largest city in the Yangtze River Delta (YRD), Eastern China, with a built-up area of 753 km^2 and a population of 8.2 million. Geographically, the YRD includes the provinces of Jiangsu, Zhejiang and Anhui and the Shanghai municipality (29.04° to 33.41° N, 118.33° to 122.95° E) with a population of 190 million. The YRD is influenced by subtropical moist monsoon climate. The mean annual temperature is about 15 ^oC and the annual precipitation is between 1000 mm and 1800 mm. The vegetation types are all C3 species. The YRD is the most industrialized region in China and had a higher urban land fraction of 10.8 % as of 2014 than the global mean (2.4 %, Akbari et al. 2009). In 2014, more than 220 large cement production factories (daily output exceeding 1000 tons) were located in the YRD (China Cement, 2016), contributing about 20 % of the national cement output.

The objectives of this study are (1) to characterize the atmospheric $\delta^{13}C$ diel, seasonal and annual variations in this urban environment, in a region where such measurement is nonexistent, (2) to investigate the influence of cement production on atmospheric $\delta^{13}C$, (3) to evaluate the performance of the Keeling plot and the Miller-Tans methods for determining δ_S, and (4) to explore the utility of the isotopic constraints for inferring the net surface flux and the plant CO_2 flux in Nanjing and in the YRD.

2 Methods

2.1 Atmospheric observation

An IRIS analyzer (model G1101-i, Picarro Inc., Sunnyvale, CA) was used to measure atmospheric CO_2 mole fraction and $^{13}C/^{12}C$ ratio ($\delta^{13}C$) continuously from February 2013 to August 2015. The analyzer was housed on the 9th floor of our laboratory building on the campus of Nanjing University of Information, Science and Technology (NUIST, 32°12' N, 118°43' E), in the northern suburb of Nanjing, at a linear distance of 20 km to the city center. The instrument inlet was at a height of 34 m above the ground. There was no large industrial CO_2 source in the 3 km radius except for a commuting road located about 300 m east of the observation site. The nearest industrial complex, the Nanjing Iron & Steel Group Co. Ltd. and the Nanjing Chemical Industry Group, was located about 5 km to the south of the site.

The measurement was made at 0.3 Hz and at an air flow rate of 30 mL min^{-1} at standard temperature and pressure. One three-way solenoid valve was combined with two two-way solenoid valves, so the analyzer could be switched for atmospheric sampling and for sampling of two standard gases. Calibration was carried out every 3 h by sampling each standard gas for 5 minutes following the procedure of Bowling et al. (2003) and Wen et al. (2013). [To avoid transient effects, only the data collected in the last 2 minutes of the 5-min calibration periods was used (Supplementary Figure S1).] Table 1 lists the concentrations and their isotopic ratios of the standard gases used in this study. These gases were balanced in air, and their concentration values bracketed the range of ambient concentration variability (Figure 3 below). Their CO_2 mole fractions were measured with a gas analyzer (model (model G1301, Picarro) and calibrated against three primary standards obtained from NOAA-

ESRL which were traceable to the WMO 2007 scale reported by the Central Calibration Laboratory of the World Meteorological Organization, and their $\delta^{13}C$ values were measured with a mass spectrometer (MAT-253, Finnigan) using IAEA reference materials IAEA-CO-8 (-5.76 ‰ VPDB) and IAEA-CO-9 (-47.32 ‰ VPDB). The mass spectrometer measurements of these reference materials were (-5.81 ± 0.04) ‰ and (-46.64 ± 0.08) ‰. The ambient measurement was averaged to hourly intervals. The isotopic ratio was expressed in the delta notation ($\delta^{13}C$) in reference to the VPDB scale.

The typical 5-min measurement precision is 0.3 ‰ for $\delta^{13}C$ and 0.05 μmol mol^{-1} for CO_2 mole fraction according to the instrument manufacturer. Our own Allan variance analysis revealed a precision of 0.05 ‰ for $\delta^{13}C$ and 0.07 μmol mol^{-1} for CO_2 mole fraction at the hourly averaging interval. These improvements were simply statistical, due to the increase in the number of samples being used for averaging. The precision of the ambient measurement was lower than this due to errors propagated through the calibration procedure. According to a laboratory test on an analyzer of the same model and using the same calibration procedure as ours, the hourly $\delta^{13}C$ precision is about 0.4 ‰ (Wen et al., 2013).

The calibration gases had much lower $\delta^{13}C$ than the ambient delta values. The mismatch in the delta value between the calibration standard and the ambient air is common in applications of the IRIS technique [$^{13}C(CH_4)$, Röckmann et al. 2016; $^{18}O(H_2O)$, Lee et al. 2005; $^{13}C(CO_2)$, Bowling et al. 2003]. For example, Bowling et al. (2003) used calibration standards with delta values of -29.55 ‰ and -40.58 ‰ to calibrate their optical $^{13}C(CO_2)$ instrument. But because the system measures the concentrations of the major and the minor isotopologue independently, it is not critical that the calibration standards and the

174 measurement target have matching isotope ratios, so long as the standards bracket
175 concentration variability of the target (Bowling et al. 2005). Nevertheless, the overall
176 accuracy of the measurement may be further improved by using calibration standards that
177 bracket variations in both the concentration and the delta values of ambient air samples.
178 We did not adopt the strict filtering technique used for background sites (Thoning et al.
179 1989) because of high natural variations in urban airsheds. We removed the first 3 min of the
180 data after switching to the ambient sampling mode from the calibration mode. Additionally,
181 data were removed if the average hourly CO_2 mole fraction was lower than 390 μmol mol^{-1}
182 (or 30 μmol mol^{-1} lower than the midafternoon value in the summer; Figure 3 below) or $\delta^{13}C$
183 were out of the range between -15 ‰ and -5.5 ‰ (or about 3 standard deviations from the
184 mean); A total of 217 hourly values were removed by these outlier criteria.
185 The $\delta^{13}C$ value measured by the analyzer in high humidity conditions is biased high due
186 to spectral broadening and direct spectral interference (Rella 2011). To correct for the
187 humidity interference, we carried out two tests using a dew-point generator (model 610, LI-
188 COR, Inc., Lincoln, NE). A CO_2 standard gas (secondary standard gas, 439 μmol mol^{-1} in test
189 one and 488 μmol mol^{-1} in test two, balanced by dry air) was fed into the dew-point
190 generator. The outlet of the dew-point generator was connected with a 3-way union with one
191 end linked to the inlet of the analyzer and the other open to the room. The humidity level of
192 the air coming out of the dew point generator was regulated at eight levels in a dew-point
193 temperature range of 1 to 30 °C, giving a water vapor mole fraction ranging from 0.66 % to
194 4.26 % (0.66 to 4.26 cmol mol^{-1}). Measurement at each humidity level lasted 30 min, with the
195 first 5 min excluded from the analysis. Because the $^{13}C/^{12}C$ ratio of the standard gas was

196 constant, any observed variations were caused by the humidity artifact. We found that no
197 correction was needed for our analyzer if the water vapor mole fraction was below 2.03 %.
198 Above this humidity level, the measurement was biased high by 0.46 ‰ for every 1 cmol
199 mol^{-1} increase in the water vapor mole fraction (Figure 1). This humidity effect is not
200 negligible, but is an order of magnitude smaller than that reported by Rella (2011). The two
201 tests, taken eight months apart, yielded essentially the same result. The correction equation is

202 $$\delta^{13}C = \delta^{13}C_{true} \qquad H_2O \leq 2.03\ \% \qquad (2a)$$

203 $$\delta^{13}C = \delta^{13}C_{true} + 0.46\ ‰\ (H_2O\ \% - 2.03\ \%) \qquad H_2O > 2.03\ \% \qquad (2b)$$

204 where H_2O is water vapor mole fraction and was measured by the same isotope analyzer,
205 $\delta^{13}C$ is the measured isotope delta value (after the two-point calibration), and $\delta^{13}C_{true}$ is the
206 true isotope delta value. The ambient vapor mole fraction varied from 0.16 to 3.64 % during
207 the measurement period. About 35 % of the observations exceeded the threshold mole
208 fraction of 2.03 % and required correction. The largest hourly correction was 0.74 ‰. In the
209 following, all the data have been corrected for the humidity interference.
210
211 **2.2 The $^{13}C/^{12}C$ ratio of surface sources (δ_S)**
212 We applied the Miller-Tans method to estimate the $^{13}C/^{12}C$ ratio of the surface source (δ_S).
213 Strictly, Equation 1 does not allow a non-zero intercept. When applied to the urban airshed in
214 Los Angles, Equation 1 does not require an intercept (Newman et al. 2016). But when applied
215 to the data obtained at the monthly time scale in this study, the regression yielded a non-zero
216 intercept (Supplementary Figure S2). To determine if a shorter time scale would improve the
217 result, we applied the 5-h moving window technique described by Vardag et al. (2016) to the

observations made in January and July 2014. Only 4 % of the data, all obtained at nighttime, satisfies their data screening criteria. The mean regression equation of this subset is y = (-26.41 ±4.03) x + (428.84 ± 211.12) for January and y = (-25.64 ±6.39) x + (687.83 ± 264.67) for July, where x is (C_a - C_b) and y is ($\delta_a C_a$ - $\delta_b C_b$). In these analyses, the background CO_2 mole fraction and the isotope ratio were those observed at Mount Waliguan (WLG, 36°17' N, 100°54' E, 3816 m above the mean sea level; https://www.esrl.noaa.gov/gmd/dv/data/index.php) located at the northeastern edge of the Tibetan Plateau (Zhou et al., 2005), the closest upwind WMO background station for Nanjing. Use of other WMO baseline sites as the background gave essentially the same results.

The selection of a background site is a critical issue when applying the Miller-Tans method (Ballantyne et al., 2011 & 2010). That the Miller-Tans intercept does not go to zero suggests that the baseline site WLG may not be a suitable background for this highly urbanized region. We tested the Miller-Tans method with other isotope data published for urban areas, and found that the intercept was nonzero for most of the urban datasets (Supplementary Figure S3 and Table S1).

In the following, we used the tropospheric CO_2 mole ratio calculated by CarbonTracker over the YRD region (altitude 3330 m; https://www.esrl.noaa.gov/gmd/dv/data/index.php) as the background concentration (C_b). The CarbonTracker mole ratio is on average 3.5 μmol mol^{-1} higher than that observed at WLG. To overcome the problem that CarbonTracker does not calculate tropospheric $\delta^{13}C$, we rearranged Equation 1 to a form that allows an intercept but without the need for a known background $\delta^{13}C$, as

$$\delta_a C_a = \delta_S (C_a - C_b) + \delta_b C_b \quad (3)$$

The $^{13}C/^{12}C$ ratio of the surface source was taken as the slope of the linear regression of $\delta_a C_a$ against $(C_a - C_b)$. A key difference between Equation 3 here and Equation 5 of Miller and Tans (2003) is that the δ_S appears only in the slope parameter in Equation 3 but in both the slope and the intercept parameter in Miller and Tans' Equation 5. This modified Miller-Tans analysis requires knowledge of background CO_2 mole fraction but not δ_b.

The Miller-Tans analysis was performed over monthly intervals, using the data collected in daytime hours (10:00 to 16:00 local time) to represent YRD and data collected during nighttime hours (22:00-6:00 local time) to represent Nanjing. Morning and evening transitional periods were omitted to avoid the confounding effects of sign change of the biological CO_2 flux and sudden changes in the atmospheric stability regime.

We interpreted the daytime results to represent the influence of surface sources in the YRD region and the nighttime results to represent the influence of surface sources in the Nanjing municipality. The vigorous turbulent exchange in the daytime boundary layer diminishes the role of local sources in the measured concentration and isotopic ratio. In other words, the daytime measurement has a much larger source footprint than the size of the urban land itself or the footprint of the nighttime measurement. In contrast, the buildup of CO_2 at night is primarily the result of sources in the city (Shen et al. 2014), so we considered the δ_S determined from the nighttime observations to represent the signal of the sources located in the city. Admittedly, this interpretation of daytime versus nighttime source areas is a simplification because the actual source area also depends on thermal stratification and

boundary layer wind. Nevertheless, it is supported by a trajectory analysis and by an analysis of the atmospheric methane to CO_2 emissions ratio (Shen et al. 2014).

For the purpose of comparing with the Miller-Tans results, we also estimated the source $^{13}C/^{12}C$ ratio using the Keeling mixing line method. According to Wehr and Saleska (2017), for the measurement uncertainties of our instrument system, the ordinary least squares procedure has much lower bias errors of parameter estimation than the geometric mean regression. In the following, the results of both the Miller-Tans method and the Keeling mixing line method were based on the ordinary least squares regression.

2.3 Inventory of anthropogenic sources

We calculated the anthropogenic CO_2 fluxes from energy consumption and industrial process following the SCOPE 1 procedure issued by the International Council for Local Environmental Initiatives (ICLEI, 2008). The procedure considers only emissions from sources that lie within the geographic boundary of investigation. The energy consumption source consists of direct emissions from the three main energy consumption sectors (industry, transport, and household). We ignored the commerce sector here because the main energy consumption in this sector in Nanjing and in the YRD was electric power generated by coal and coal consumption which was already considered in SCOPE 1. The amounts of CO_2 emission were estimated with the IPCC methodology adopting the emission factors for each fossil fuel type recommended by IPCC. The calculations were done separately for the YRD region and for the Nanjing municipality. Because no statistical data were available for energy consumption in the transport sector in Nanjing, the CO_2 emission from the transport sector

283 was deduced according to vehicle number, average annual driving distance and coefficients
284 of fuel economy (Bi et al. 2011). We obtained the data on energy consumption from official
285 sources (CESY 2013, CSY 2013, NSY, 2013).
286 The non-energy industrial processes included cement, raw iron, crude steel, and
287 ammonia synthesis processes. In the YRD, the data were available at monthly intervals. For
288 the city of Nanjing, only annual statistics were available.
289
290 **2.4 Partitioning the net surface flux**
291 We partitioned the surface CO_2 flux (F_S) into three component fluxes according to the
292 following mass conservation equations
293 $$F_S = F_F + F_C + F_P \quad (4)$$
294 $$\delta_S F_S = \delta_F F_F + \delta_C F_C + \delta_P F_P \quad (5)$$
295 where F_F is the flux from fossil fuel combustion and industrial emission except cement
296 production (termed "fossil plus"), F_C is the flux due to cement production, F_P is the biological
297 flux, and δ_F, δ_C, and δ_P are the $\delta^{13}C$ value of F_F, F_C and F_P, respectively. These CO_2 mass
298 fluxes are obtained by dividing the total emission by the surface area within the geographic
299 boundary of Nanjing or the YRD, having dimensions of mg m^{-2} s^{-1}. We separated the cement
300 source from other non-energy consumption industrial processes because its $^{13}C/^{12}C$ ratio is
301 much higher. In these equations, the monthly net surface flux (F_S) and the biological flux (F_P)
302 are unknowns to be solved for, and all other terms are either provided by the atmospheric
303 measurement or by the inventory calculation. The partitioning analysis was done for both
304 Nanjing and the YRD using the nighttime and daytime observations, respectively.

305 The value for δ_F was the weighted average of the isotope ratio of individual fuel types
306 and industrial processes (Table 2). The delta value of CO_2 from cement production is
307 provided by Anders (1994). We adopt a value of (-28.2 ‰) for δ_P for the YRD and Nanjing,
308 on account of a linear relationship between δ_P and tree age (Fessenden and Ehleringer 2002),
309 a typical tree age in this region (40 years) and a U-shaped relationship between δ_P and annual
310 precipitation (Pataki et al. 2007). Our δ_P is more negative than that reported for a boreal forest
311 (-26.2 ‰; Pataki et al. 2007) but is in closer agreement with the value reported for a Ginkgo
312 tree in Nanjing (-29.3 ‰; Sun et al. 2003). A summary of the isotopic ratios of the four
313 source categories is given in Table 3.
314 Uncertainties in the delta values of the different fuel types and industrial processes were
315 based on the data found in the references listed in Table 2. The uncertainty in δ_P was assumed
316 to be ± 1.00 ‰ (Verdag et al. 2016). The mass flux terms F_F and F_C were assumed to have a
317 10% uncertainty, which is typical of fossil fuel consumption data (Vardag et al. 2016).
318 To partition the nighttime flux for Nanjing, we assumed that the nighttime F_F was 20 %
319 of the daily value. The parameter 20 % was determined by the diel variation of the CO_2 flux
320 observed with an eddy covariance system in Nanjing (Bai 2011) and in several other cities
321 (Coutts et al. 2007, Song and Wang. 2011, Liu et al. 2012). At night, most of the factories in
322 the city were closed and the traffic flow was reduced to about 80 % of the daytime volume
323 (Yang et al. 2011).
324 The partitioning equations are explicit expressions of the mass balance principle. But
325 uncertainties in the isotope delta end members and the anthropogenic fluxes can propagate
326 through these equations, causing uncertainties in the estimation of F_S and F_P. Here we used a

Monte Carlo analysis to quantify the error propagation. The same analysis has been applied to the partitioning of lake water budgets from isotope end members (Jasechko et al. 2014). The procedure employed a Gaussian distribution for errors in the input variables and an ensemble of 10,000 realizations for each month. Errors in F_S and F_P were computed as one standard deviation of these realizations after excluding the top and bottom 50 extreme ensemble members.

3. Results

3.1. Temporal variations in the CO_2 mole fraction and $\delta^{13}C$

The monthly CO_2 mole fraction during the summer was slightly lower than in the other seasons (Figure 2). The mean mole fraction was 446.7 μmol mol^{-1} and 431.1 μmol mol^{-1} for January and July, respectively, giving a seasonal amplitude of 15.6 μmol mol^{-1}. The mean CO_2 mole fraction during the whole experimental period (March 2013 to August 2015) was 439.7 μmol mol^{-1}, which is 40.6 μmol mol^{-1} higher than the value observed at WLG for the same period. In 2014, the calendar year with complete data coverage, the mean CO_2 mole fraction was 441.2 μmol mol^{-1}, which is 42.5 ppm higher than the WLG value for the same year.

The $^{13}C/^{12}C$ ratio of atmospheric CO_2 displayed a more clear seasonal cycle than the mole fraction (Figure 2). The monthly mean value was (-9.07 ± 0.17) ‰ (mean ± standard error) and (-7.63 ± 0.18) ‰ for January and July, respectively, with a seasonal amplitude of 1.44 ‰. The mean value for the whole experimental period was -8.48 ‰, which is the same as the WLG value (-8.48 ‰). The summertime (June to August) $\delta^{13}C$ was 0.39 ‰ higher than

the WLG background value. The seasonality of the $^{13}C/^{12}C$ ratio at Nanjing was greater than that at WLG.

The strongest diel variation in the CO_2 mole fraction was observed in the autumn season (September to November) and the weakest in the winter season (December to February), with a diel amplitude of 27.9 μmol mol^{-1} and 13.4 μmol mol^{-1}, respectively (Figure 3). In the summer season, the peak value was observed at 07:00 and the lowest value at 19:00. In contrast to the CO_2 mole fraction, $\delta^{13}C$ showed the lowest value in the early morning and the highest value in the afternoon in all the four seasons. The diel amplitude was 1.36 ‰ in the summer and 0.66 ‰ in the winter.

3.2 $^{13}C/^{12}C$ ratio of the surface sources (δ_S)

Figures 4 and 5 show an example of the modified Miller-Tans approach applied to the month of January 2014. According to the slope parameter estimation, the $^{13}C/^{12}C$ ratio of the surface sources was (-25.01 ± 0.90) ‰ (mean ± 95 % confidence limit) for the YRD (Figure 4) and (-25.23 ± 0.74) ‰ for Nanjing (Figure 5).

Figure 6 shows the monthly isotopic ratio calculated with the Miller-Tans method for the whole observation period. The reader is reminded here that the results obtained for the daytime and the nighttime period represent sources in the YRD and in Nanjing, respectively. During the two and a half years of observation, the monthly δ_S for the YRD was lower in the winter [(-24.37 ± 0.71) ‰] and higher in the summer (-23.42 ± 1.79 ‰]. The seasonal difference for Nanjing was smaller than for the YRD [(-24.87 ± 0.51) ‰ in the winter (December to February) and -24.80 ± 1.79) ‰ in the summer months (June to August)]. The

371 sources in the YRD had slightly higher δ_S than those in in Nanjing. The mean δ_S value of the
372 whole observational period was (-24.37 ± 0.61) ‰ and (-24.58 ± 0.44) ‰ for the YRD and
373 Nanjing, respectively. The monthly δ_S for the YRD (Figure 6a) was highly correlated with the
374 monthly atmospheric $\delta^{13}C$ [Figure 2; $\delta_S = (2.29 \pm 0.78)\ \delta^{13}C + (-5.71 \pm 6.37)$, linear correlation
375 coefficient = 0.47, n = 30, $p < 0.01$]. The correlation between the monthly δ_S for Nanjing
376 (Figure 6b) and the monthly atmospheric $\delta^{13}C$ was weak [$\delta_S = (2.39 \pm 0.92)\ \delta^{13}C + (-3.71 \pm$
377 8.07), linear correlation coefficient = 0.03, n = 30, p = 0.87]. These correlation patterns
378 suggest that atmospheric $\delta^{13}C$ was influenced more by surface sources at the regional scale
379 than at the local (city) scale.
380
381 **3.3 Inventory data for anthropogenic sources**
382 The emission strength of anthropogenic sources and their $^{13}C/^{12}C$ ratios were calculated with
383 the inventory method and the data found in the literature, as described in section 2.3. In the
384 YRD, coal combustion was by far the largest source of anthropogenic CO_2, contributing 70 %
385 of the overall "fossil-plus" emission (Table 2). Here the "fossil-plus" emission includes
386 contributions from all forms of fossil fuel combustion and from non-cement industrial
387 processes. The second and third largest source were ammonia synthesis and pig iron
388 manufacturing, with fractional contributions of about 9 %. The "fossil-plus" source
389 contribution to the total anthropogenic emission was 91 %, with the remaining 9 %
390 contributed by cement production (Table 2).
391 In the Nanjing municipality, the fractional contribution of coal to the "fossil-plus" total
392 was 52 %, lower than that for the YRD, and the other three major sources were ammonia

393 synthesis (16 %), pig iron (13 %), and gasoline (11 %). The fractional contribution of fuel-
394 plus sources to the total anthropogenic emission was 96.4 % and the fractional contribution of
395 cement production was 3.6 % (Table 2). The isotopic ratio of the "fossil-plus" sources was
396 0.35 ‰ lower for Nanjing than for the YRD.

397 The overall effective isotopic ratio of the anthropogenic sources weighted by the source
398 contributions was also lower for Nanjing than for the YRD (Table 3). The difference was
399 1.76 ‰ and was a result of lower fractional contributions in Nanjing of coal combustion and
400 cement production, which have relatively high ^{13}C contents, and a higher fractional
401 contribution of natural gas, which is the fuel type with the lowest ^{13}C content.

402

403 **3.4. CO_2 fluxes in YRD and Nanjing**

404 Figure 7 shows the biological flux F_P and surface flux F_S calculated from the mass balance,
405 and the cement flux F_C and "fossil-plus" F_F. The F_P flux obtained with the isotopic
406 partitioning method for the YRD agreed with the seasonal phenology expected for plants in
407 this region. It was near zero or slightly negative in the summer and generally positive in the
408 winter, indicating uptake and release, respectively. The annual mean daytime biological flux
409 was (0.03 ± 0.64) mg m^{-2} s^{-1} in the YRD in the calendar year 2014. The net surface flux F_S
410 was (0.17 ± 2.02) mg m^{-2} s^{-1} in 2014. The standard deviations of these estimates are quite
411 large. If the extreme standard deviations of F_P (5.16 mg m^{-2} s^{-1}) and F_S (22.00 mg m^{-2} s^{-1}) in
412 March 2014 were excluded, the mean standard deviation of F_P would decrease to 0.23 mg m^{-2}
413 $s^{-1}$for and that of F_S to 0.20 mg m^{-2} s^{-1}.

In Nanjing, the biological flux was positive throughout the year (Figure 8). This is because the partitioning was done for the night hours when the natural ecosystems were a source of CO_2 due to autotrophic and heterotrophic respiration. The annual mean nighttime biological flux for the calendar year 2014 was (0.06 ± 0.26) mg m^{-2} s^{-1}. The nighttime surface flux was (0.18 ± 0.22) mg m^{-2} s^{-1} in 2014.

4 Discussion

4.1 CO_2 mole fraction and $\delta^{13}C$ seasonality

The atmospheric CO_2 mole fraction observed in Nanjing showed very small seasonal variation (summer versus winter difference of 7.9 μmol mol^{-1}, July versus January difference of 15.6 μmol mol^{-1}), in comparison with the data published for other cities. For example, in Salt Lake City, USA, the CO_2 mole fraction in the summer is about 31 μmol mol^{-1} lower than in the winter (Pataki et al., 2003). Several factors contributed to the weak seasonality in Nanjing. The climate in the YRD is relatively mild. The governmental energy policy prohibits winter heating in public buildings. Most residential buildings also lack space heating in the winter. This is in contrast to energy use patterns in northern cities in China and elsewhere. The weak seasonality of the observed mole fraction was also related to the low vegetation cover in the YRD and in Nanjing. The forest cover ratio is about 35 % in Nanjing and in the YRD, and the overall vegetation cover (forest plus other vegetation types) ratio in the major cities in the YRD is lower than 45 % (CESY, 2013; CSY, 2013). For comparison, the vegetation cover ratio is 56 % in Salt Lake City (Pataki et al. 2009) and 44 % in Chicago

435 (Rose et al. 2003). Dense vegetation is known to deplete atmospheric CO_2 in the summer
436 season via photosynthetic uptake, amplifying the CO_2 seasonal amplitude.
437 Our $\delta^{13}C$ seasonal amplitude (January versus July difference of 1.44 ‰) was 4 times the
438 amplitude observed or estimated at WLG (Figure 2) but agreed with those reported by most
439 urban studies. For comparison, the seasonal amplitude of $\delta^{13}C_a$ in Bangalore, India, was 0.89
440 to 1.32 ‰ (Guha and Ghosh 2015). Similar amplitudes have also been reported for Chicago
441 (January versus August difference of 1.25 ‰; Moore and Jacobson, 2015) and Beijing
442 (2.13 ‰; Pang et al. 2016). In Salt Lake City, the seasonal amplitude of $\delta^{13}C$ was
443 approximately 1.6 ‰ because of much more natural gas consumption for heating in the
444 winter than in the summer (Pataki et al. 2006).
445
446 **4.2 Influences of cement production on atmospheric $\delta^{13}C$**
447 The high summer $\delta^{13}C$ was one of the most unique characteristics at our site. The daytime
448 $\delta^{13}C$ reached -6.90 ‰ in July 2013 and -7.21 ‰ in August 2014, which were 1.28 ‰ and
449 0.95 ‰ higher than the WLG values. The highest monthly mean $\delta^{13}C$ occurred in July: -
450 7.44 ‰ in July 2013, -7.99 ‰ in July 2014 and -7.46 ‰ in July 2015. These values were
451 0.74 ‰, 0.16 ‰ and 0.77 ‰ higher than the WLG value reported for the same months.
452 The high July values observed at our site cannot be fully explained by CO_2 removal by
453 plant photosynthesis. Photosynthesis and respiration are the two processes that dominate the
454 $^{13}C/^{12}C$ seasonality in plant-dominated landscapes, leading to higher $\delta^{13}C$ values in the
455 summer and lower values in the winter. For example, in Park Falls, Wisconsin, USA, a site in
456 a heavily-forested landscape, $\delta^{13}C$ was -7.75 ‰ in August 2011 and -8.77 ‰ in February

2012 (Moore and Jacobson, 2015). For comparison, $\delta^{13}C$ was -8.24‰ and -8.38 ‰ at the Mauna Loa Observatory and -8.02 ‰ and -8.66 ‰ at WLG in these two months, respectively. In other words, the photosynthetic effect raised the August $\delta^{13}C$ by 0.5 ‰ above the background value, a smaller enrichment than observed at our site. Because of the low vegetation fraction, the summer photosynthetic CO_2 uptake in the YRD and in Nanjing should be lower than at Park Falls. According to the CarbonTracker inversion analysis (Peters et al. 2007), the net ecosystem production at the grid point where Parks Fall is located is -0.201 mg m^{-2} s^{-1} in July, 2014 but is only -0.059 mg m^{-2} s^{-1} at the grid point corresponding to the YRD region. We would expect from the photosynthetic effect alone that the summertime ^{13}C enrichment at our site to be smaller, not greater than that observed at Park Falls.

Furthermore, in a human-dominated landscape, the plant photosynthetic enhancement of ^{13}C is offset by the CO_2 from fossil fuel combustion which has lower $^{13}C/^{12}C$ ratios than the atmosphere. In Chicago, the monthly mean $\delta^{13}C$ peaked in August at -8.29 ‰ during the calendar year 2011, which is 0.05 ‰ lower than the WLG value for the same month. Similarly, in Beijing, the monthly mean $\delta^{13}C$ peaked at -9.49 ‰ in August 2014, which is 1.23 ‰ lower than the WLG value for the same month.

We suggest that cement production was the contributing factor responsible for the high $\delta^{13}C$ values in the summer. The evidence supporting this interpretation is provided by data in Table 3 and Figure 7. The delta value of anthropogenic CO_2 in the YRD would be (-26.36 ± 0.42) ‰ without cement production and increased to (-23.95 ± 0.41) ‰ after inclusion of the cement source (Table 3). This value is much higher than those reported for other urban lands, such as -30.7 ‰ for Los Angeles, USA (Newman et al. 2008) and about -31 ‰ for Salt Lake

479 City, USA (Bush et al. 2007). The overall surface source $^{13}C/^{12}C$ ratio derived from
480 atmospheric measurements (Figure 6; -24.37 ‰ and -24.58 ‰ for the YRD and Nanjing,
481 respectively) was also more enriched than those obtained from atmospheric measurements in
482 other cities, such as (-28.1 ± 0.8) ‰ for Chicago in August and September (Moore and
483 Jacobson, 2015), -32.4 ‰ to -27.4 ‰ for Salt Lake City in the growing season (Pataki et al.
484 2003), -27.0 ‰ for Beijing in the winter heating season (Pang et al. 2016), and -29.3 ‰ for
485 Los Angeles, USA (Newman et al. 2008).
486 The influence of cement production on atmospheric $\delta^{13}C$ has also been suggested for at
487 least two other urban sites. In Bangalore, India, $\delta^{13}C$ is 0.05 ‰ higher than that observed at
488 an island station in the Indian Ocean, and cement production in southern India is offered as a
489 reason to explain the enrichment of urban $\delta^{13}C$ (Guha and Ghosh 2015). The other urban site
490 is Beijing, China, where the $\delta^{13}C$ measurement may have been influenced by cement factories
491 outside the city (Ren et al. 2015, Pang et al. 2016).
492
493 **4.3 Net surface and biological fluxes in the YRD**
494 As a human-dominated landscape, the YRD was a net source of CO_2 on the monthly scale
495 even in the growing season (F_S, Figure 7). The seasonal trends of the net surface flux F_S and
496 the biological flux F_P were highly correlated with each other ($R^2 = 0.88$ after exclusion of
497 three extreme outliers) because the anthropogenic source strengths were almost constant. The
498 mean F_S between March 2013 and February 2015 was (0.19 ± 1.16) mg m^{-2} s^{-1}, which
499 consisted of (0.15 ± 0.02) mg m^{-2} s^{-1} from fossil combustion and industrial processes, (0.02 ±
500 0.002) mg $m^{-2}s^{-1}$ from cement production and (0.05 ± 1.31) mg m^{-2} s^{-1} from biological

activities. The total anthropogenic CO_2 flux was (0.17± 0.02) mg m^{-2} s^{-1} in the YRD, a 70 % increase from the value of 0.10 mg m^{-2} s^{-1} reported for 2009 (Shen et al. 2014). From 2009 to 2012, the GDP increased by 56 % according to the National Statistic Yearbook.

For comparison, we extracted the flux data from the CarbonTracker database for the 6 by 6 pixels that cover the YRD region. The results show that the mean daytime (11:00 to 17:00 local time) biological flux is slightly negative at -0.01 mg m^{-2} s^{-1} for 2014 (Peter et al. 2007). Our estimate of F_P for 2014 was (0.03 ± 0.64) mg m^{-2} s^{-1}. As pointed out earlier, the F_p value for March 2014 was highly uncertain [(0.21± 5.16) mg m^{-2} s^{-1}]; If we replace this value by the mean value of February and April 2014, the 2014 mean F_P would be reduced to (0.02 ± 0.22) mg m^{-2} s^{-1}.

A source of uncertainty in our flux partitioning analysis is related to human breath (Affek and Eiler 2006). Using the method of Prairie and Duarte (2007), we estimated that human respiration flux was 0.006 and 0.013 mg m^{-2} s^{-1}, or 3.7 % and 11.65 % of anthropogenic emission in the YRD and in Nanjing, respectively. The food diet in the region is predominantly C3 grains. By including this additional source in Equations 3 and 4 and by assuming that the isotopic ratio of digestion is the same as δ_P shown in Table 3, F_S and F_P would increase by 0.008 and 0.001 mg m^{-2} s^{-1} in the YRD and by 0.018 mg m^{-2} s^{-1} and 0.005 mg m^{-2} s^{-1} in Nanjing, respectively.

4.4 Comparison of the Miller-Tans and the Keeling methods

By applying the Miller-Tans method to daytime and nighttime observations separately, we obtained the effective source ratios that are consistent with the inventory analysis for the

YRD and for the Nanjing Municipality. The daytime measurement (Figure 6a, solid circles) revealed that the $^{13}C/^{12}C$ ratio of the all sources (anthropogenic and biological) was on average 0.21 ‰ higher than that obtained with the nighttime measurement (Figure 6b, solid circles), although the difference is not statistically significant (p = 0.38). For comparison, the overall δ_S of the anthropogenic sources in the YRD was also higher than that in Nanjing, the difference being 2.01 ‰ (Table 3). The interpretation that the daytime observations capture the influence of surface sources in the YRD region is supported by a trajectory analysis and by an analysis of the atmospheric methane to CO_2 emissions ratio observed at the same site (Shen et al. 2014). We note that the atmospheric measurements gave a smaller difference between the YRD and Nanjing than that obtained by the inventory data, likely because of different biological contributions between the two spatial scales.

One open question with regard to the modified Miller-Tans method is what constitutes the true background air for the YRD. In this study, the background was assumed to be the tropospheric air above the YRD. The background delta value (δ_b) backed out from the intercepts shown in Figures 4 and 5 is -7.6 ‰, which is higher than expected, suggesting that the true background concentration C_b may be higher than the tropospheric value. One noteworthy feature about Equation 3 is that its slope parameter is not sensitive to C_b, but its intercept parameter is. By increasing C_b by 15 μmol mol^{-1}, the slope of the regression in Figure 5 would remain unchanged, but the δ_b backed out from the new intercept value would become more reasonable (-8.23 ‰). In Newman et al. (2016), the background air was measured at a coastal location upwind of the Los Angles airshed. It is recommended that a similar strategy should be used in future experiments, where simultaneous measurement is

545 made at the coast of East China Sea and only data collected in easterly winds are selected for
546 the Miller-Tans analysis.

547 We also calculated the $^{13}C/^{12}C$ ratio of the surface sources with the Keeling plot method.
548 Using the daytime data, the Keeling result was lower and more variable than that inferred
549 from the Miller-Tans method using the daytime data (Figure 6a). The two methods differed
550 by an average of -1.51 ‰ (Supplementary Table S2).

551 In comparison, the Keeling plot method showed reasonably good performance when
552 applied to the nighttime observations. This is because surface inversion conditions effectively
553 prevented mixing of the free atmospheric air with the surface air, so that the single-source
554 assumption implicit in the Keeling plot method could be satisfied. When we applied Keeling
555 plot method at monthly intervals to the nighttime data, the resulting δ_S showed very similar
556 month-to-month variations with the value obtained with application of the Miller-Tans
557 method to the nighttime observations (Figure 6b). The two method differed by an average of
558 1.21 ‰ (Supplementary Table S2).

559 When the δ_S derived from the Keeling plot method was used for flux-partitioning, the
560 results were much more erratic than shown in Figures 7 and 8 (Supplementary Figures S3 and
561 S4). The uncertainty ranges of the monthly F_P and F_S were two to three times larger. The
562 biological flux F_P for the YRD was out of range for 4 months, and did not display an obvious
563 seasonal pattern (Supplementary Figure S3). These results support our choice of the modified
564 Miller-Tans method as the preferred approach for inferring the overall $^{13}C/^{12}C$ ratio of the
565 surface sources in this study.
566

5. Conclusion

We showed that the temporal changes of $\delta^{13}C$ followed the seasonal patterns of anthropogenic and biologic CO_2 emissions, with lower values in the winter than in the summer. An unusual feature that has not been seen in other urban environments is that the $\delta^{13}C$ exceeded that of the background atmosphere in some of the summer months. The highest monthly $\delta^{13}C$ was -7.44 ‰ observed in July 2013, which was 0.74 ‰ greater than the WLG value for the same month. Evidence points to cement production as the key reason for why the atmospheric $\delta^{13}C$ was higher than at the background site. In contrast to the isotope ratio, the CO_2 mole fraction displayed very weak seasonality (July to January difference 15.6 μmol mol^{-1}).

We hypothesized that the Miller-Tans method applied to the daytime and nighttime observations should yield the effective $^{13}C/^{12}C$ ratio of surface sources at the regional (YRD) and the local (Nanjing) scale, respectively. According to the results of the modified Miller-Tans method, the effective source $^{13}C/^{12}C$ ratio in the YRD was -24.37 ‰, which was 0.21 ‰ higher than that in the Nanjing Municipality. These results were consistent with inventory estimates of anthropogenic source ratios at these two spatial scales.

By combining inventory data on anthropogenic carbon sources and the atmospheric measurement of CO_2 mole fraction and $^{13}C/^{12}C$ ratio in an isotopic partitioning framework, we inferred that natural ecosystems in the YRD were a negligibly small source of atmospheric CO_2, with an average flux of (0.02 ± 0.22) mg m^{-2} s^{-1} for 2014. For comparison, the CarbonTracker inverse analysis reveals a small annual mean daytime biological flux (-0.01 mg m^{-2} s^{-1}) for this region for 2014.

Data availability:

The atmospheric data are available upon request and from the Yale-NUIST Center website http://yncenter.sites.yale.edu/publications.

Acknowledgments:

This research was supported by the National Natural Science Foundation of China (Grant 41475141, 41505005), the U. S. National Science Foundation (Grant 1520684), the Ministry of Education of China (Grant PCSIRT), and the Priority Academic Program Development of Jiangsu Higher Education Institutions (Grant PAPD). The first author also acknowledged a visiting scholarship from China Scholarship Council and a Graduate Student Innovation Grant from Jiangsu Provincial Government (Grant KYLX_0848). We thank the handling editor Dr. Jan Kaiser and four anonymous reviewers whose constructive comments have greatly improved this paper.

References

Affek, H. P., Eiler, J. M. (2006). Abundance of mass 47-CO_2 in urban air, car exhaust, and human breath. Geochimica et Cosmochimica Acta **70**(1): 1-12.

Akbari H, Menon S, Rosenfeld A. Global cooling: increasing world-wide urban albedos to offset CO_2. Climatic Change, 2009, **94**(3-4): 275-286.

An, H (2012) Ammonia synthesis: current status and future outlook (in Chinese), Coal Chemsitry of Western China, **2**: 4-13.

Andres, R. J., Marland, G., Boden, T., Bischof, S. (1994). Carbon dioxide emissions from fossil fuel consumption and cement manufacture, 1751-1991; and an estimate of their isotopic composition and latitudinal distribution, Oak Ridge National Lab., TN (United States);

Bai, Y., (2011) A Comparative Study on Turbulent Fluxes Exchange over Nanjing Urban and Suburban in Summer (in Chinese), Master's Thesis, Nanjing University of Information Science & Technology.

Ballantyne, A. P., Miller, J. B., Baker, I. T., Tans, P. P., White, J. W. C. (2011). Novel applications of carbon isotopes in atmospheric CO_2: what can atmospheric measurements teach us about processes in the biosphere? Biogeosciences, 8(10), 3093-3106.

Ballantyne, A. P., Miller, J. B., Tans, P. P. (2010). Apparent seasonal cycle in isotopic discrimination of carbon in the atmosphere and biosphere due to vapor pressure deficit. Global Biogeochemical Cycles, 24(3), 1-16.

Bowling, D. R., S P Burns, T. J. Conway, R. K. Monson, and J. W. C. White (2005) Extensive observations of CO_2 carbon isotope content in and above a high-elevation subalpine forest, Global Biogeochemical Cycles, **19**: GB3023.

Bi, J., Zhang, R., Wang, H., Liu, M.,Wu, Y. (2011). The benchmarks of carbon emissions and policy implications for China's cities: Case of Nanjing. Energy Policy **39**(9): 4785-4794.

Bowling, D. R., Sargent, S. D., Tanner, B. D., and Ehleringer, J. R. (2003). Tunable diode laser absorption spectroscopy for stable isotope studies of ecosystem–atmosphere CO_2 exchange, Agric. Forest Meteorol., **118:** 1–19.

Bush, S. E., Pataki, D.E., Ehleringer, J.R. (2007). Sources of variation in $\delta^{13}C$ of fossil fuel emissions in Salt Lake City, USA. Applied Geochemistry **22**(4): 715-723.

CESY (2013). China Energy Statistical Yearbook 2013: China Statistical Publishing House, Beijing. (in Chinese) Also available at: <http://www.stats.gov.cn/tjsj/ndsj/2013/indexch.htm>.

Clark-Thorne, S. T., C. J. Yapp (2003). Stable carbon isotope constraints on mixing and mass balance of CO2 in an urban atmosphere: Dallas metropolitan area, Texas, USA. Applied Geochemistry **18**(1): 75-95.

Coutts, A. M., Beringer, J., Tapper, N.J. (2007). Characteristics influencing the variability of urban CO_2 fluxes in Melbourne, Australia. Atmospheric Environment **41**(1): 51-62.

China Cement: http://hy.ccement.com/map/, last access: 6 July 2016 (in Chinese).

CSY (2013). China Statistical Yearbook. National Bureau of Statistics of China. (in Chinese) Also available at: <http://www.stats.gov.cn/tjsj/ndsj/2013/indexch.htm>

Duan Y. (1995) Study of characteristics of coal isotope conposition in China. Coal Geology & Exploration **23**(1) 29-33.

Ehleringer, J.R., Bowling, D.R., Flanagan, L.B., Fessenden, J.,Helliker, B., Martinelli, L.A., Ometto, J.P. (2002). Stable isotopes and carbon cycle processes in forests and grasslands. Plant biology **4**(2): 181-189.

Farquhar, G., J. Lloyd (1993). Carbon and oxygen isotope effects in the exchange of carbon dioxide between terrestrial plants and the atmosphere. Stable isotopes and plant carbon-water relations **40**: 47-70.

Fessenden, J. E., J. R. Ehleringer (2002). Age-related variations in $\delta^{13}C$ of ecosystem respiration across a coniferous forest chronosequence in the Pacific Northwest. Tree Physiology **22**(2-3): 159-167.

Friedman, L., A. P. Irsa (1967). Variations in isotopic composition of carbon in urban atmospheric carbon dioxide. Science **158**(3798): 263-264.

Gorski G, Strong C, Good S P, Bares, R., Ehleringer, J. R., Bowen, G. J. (2015). Vapor hydrogen and oxygen isotopes reflect water of combustion in the urban atmosphere. Proceedings of the National Academy of Sciences, **112**(11): 3247-3252.

Griffis, T. J., Lee, X., Baker, J.M., Sargent, S.D., King, J.Y. (2005). Feasibility of quantifying ecosystem–atmosphere $C^{18}O^{16}O$ exchange using laser spectroscopy and the flux-gradient method. Agricultural and Forest Meteorology, **135**(1-4): 44-60.

686 Griffis, T J. (2013). Tracing the flow of carbon dioxide and water vapor between the
687 biosphere and atmosphere: A review of optical isotope techniques and their application.
688 Agricultural and Forest Meteorology, **174**:85-109.
689
690 Guha, T., P. Ghosh (2010). Diurnal variation of atmospheric CO_2 concentration and delta C-
691 13 in an urban atmosphere during winter-role of the nocturnal boundary layer. Journal of
692 Atmospheric Chemistry, **65**(1): 1-12.
693
694 Guha, T. and P. Ghosh (2015). Diurnal and seasonal variation of mixing ratio and delta C-13
695 of air CO_2 observed at an urban station Bangalore, India. Environmental Science and
696 Pollution Research, **22**(3): 1877-1890.
697
698 ICLEI (International Council for Local Environmental Initiatives). (2008). Local government
699 operations protocol for the quantification and reporting of greenhouse gas emissions
700 inventories. [Available online at http://www.arb.ca.gov/cc/protocols/localgov/archive/final
701 lgo protocol 2008–09–25.pdf.]
702
703 Jasechko, S., Gibson, J. J., Edwards, T. W. (2014). Stable isotope mass balance of the
704 Laurentian Great Lakes. Journal of Great Lakes Research, **40**(2), 336-346.
705
706 Jasek, A., Zimnoch, M., Gorczyca, Z., Smula, E., Rozanski, K. (2014). Seasonal variability of
707 soil CO2 flux and its carbon isotope composition in Krakow urban area, Southern Poland.
708 Isotopes in Environmental and Health Studies, **50**(2): 143-155.
709
710 Keeling, C. D. (1958). The concentration and isotopic abundances of atmospheric carbon
711 dioxide in rural areas. Geochimica et Cosmochimica Acta, **13**(4): 322-334.
712
713 Keeling, C. D. (1961). The concentration and isotopic abundances of carbon dioxide in rural
714 and marine air. Geochimica et Cosmochimica Acta, **24**(3): 277-298.
715
716 Koerner, B., J. Klopatek (2002). Anthropogenic and natural CO_2 emission sources in an arid
717 urban environment. Environmental Pollution, **116**: S45-S51.
718
719 Leavitt, S. W., Paul, E.A., Galadima, A., Nakayama, F.S., Danzer, S.R., Johnson, H., Kimball,
720 B.A. (1995). Carbon isotopes and carbon turnover in cotton and wheat FACE experiments.
721 Plant and Soil **187**(2): 147-155.
722
723 Lee, X., Sargent, S., Smith, R., & Tanner, B. (2005). In situ measurement of the water vapor
724 $^{18}O/^{16}O$ isotope ratio for atmospheric and ecological applications. Journal of Atmospheric and
725 Oceanic Technology, **22**(5), 555-565.
726
727 Lichtfouse, E., Lichtfouse, M., Jaffrezic, A. (2003). delta C-13 values of grasses as a novel
728 indicator of pollution by fossil-fuel-derived greenhouse gas CO_2 in urban areas.
729 Environmental Science & Technology, **37**(1): 87-89.

Liu, H., Feng, J., Järvi, L., Vesala, T. (2012). Four-year (2006–2009) eddy covariance measurements of CO_2 flux over an urban area in Beijing. Atmospheric Chemistry and Physics, **12**(17): 7881-7892.

Lloyd, J., Kruijt, B., Hollinger, D.Y., Grace, J., Francey, R.J., Wong, S., Kelliher, F.M., Miranda, A.C., Farquhar, G.D., Gash, J.H.C. (1996). Vegetation effects on the isotopic composition of atmospheric CO_2 at local and regional scales: theoretical aspects and a comparison between rain forest in Amazonia and a boreal forest in Siberia. Functional Plant Biology, **23**(3): 371-399.

Lloyd, J., Francey, R.J., Mollicone, D., Raupach, M.R, Sogachev, A., Arneth, A., Byers, J.N., Kelliher, F.M., Rebmann, C., Valentini, R. (2001). Vertical profiles, boundary layer budgets, and regional flux estimates for CO_2 and its $^{13}C/^{12}C$ ratio and for water vapor above a forest/bog mosaic in central Siberia. Global Biogeochemical Cycles, **15**(2): 267-284.

McDonald, B.C., McBride, Z. C., Martin, E. W., Harley, R. A. (2014). High-resolution mapping of motor vehicle carbon dioxide emissions. Journal of Geophysical Research: Atmospheres, **119**(9): 5283-5298.

McManus, J. B., Zahniser, M.S., Nelson, D.D., Williams, L.R., Kolb, C.E. (2002). Infrared laser spectrometer with balanced absorption for measurement of isotopic ratios of carbon gases. Spectrochimica Acta Part A: Molecular and Biomolecular Spectroscopy, **58**(11): 2465-2479.

Miller, J. B., P. P. Tans (2003). Calculating isotopic fractionation from atmospheric measurements at various scales, Tellus B, **55**(2): 207-214.

Miller, J.B., Tans, P.P., White, J.W.C., Conway, T.J., Vaughn, B.W. (2003). The atmospheric signal of terrestrial carbon isotopic discrimination and its implication for partitioning carbon fluxes, Tellus B, **55**(2): 197-206.

Moore J., Jacobson A.D. (2015). Seasonally varying contributions to urban CO_2 in the Chicago, Illinois, USA region: Insights from a high-resolution CO_2 concentration and $d^{13}C$ record. Elementa: Science of the Anthropocene, **3**: 000052.

Mu, H., Li, H., Zhang, M., Li, M. (2013). Analysis of China's carbon dioxide flow for 2008. Energy Policy **54**: 320-326.

Newman, S., Xu, X., Gurney, K.R., Hsu, Y.K., Li, K.F., Jiang, X., Keeling, R., Feng, S., O'Keefe, D., Patarasuk, R. and Wong, K.W. (2016). Toward consistency between trends in bottom-up CO_2 emissions and top-down atmospheric measurements in the Los Angeles megacity. Atmospheric Chemistry and Physics, **16**(6):3843-3863.

Newman, S., Xu, X., Affek, H.P., Stolper, E., Epstein, S. (2008). Changes in mixing ratio and isotopic composition of CO2in urban air from the Los Angeles basin, California, between 1972 and 2003, Journal of Geophysical Research, **113**(D23): 1-15.

NSY (2013). Nanjing Statistical Yearbook. Nanjing Municipal Bureau Statistics. (in Chinese) Also available at: < http://www.njtj.gov.cn/2004/2013/renmin/index.htm>

Ometto, J. P., Flanagan, L.B., Martinelli, L.A., Moreira, M.Z., Higuchi, N., Ehleringer, J.R. (2002). Carbon isotope discrimination in forest and pasture ecosystems of the Amazon Basin, Brazil, Global Biogeochemical Cycles, **16**(4):1-10.

Ometto, J.P., Ehleringer, J.R., Domingues, T.F., Berry, J.A., Ishida, F.Y., Mazzi, E., Higuchi, N., Flanagan, L.B., Nardoto, G.B., Martinelli, L.A. (2006). The stable carbon and nitrogen isotopic composition of vegetation in tropical forests of the Amazon Basin, Brazil, Biogeochemistry, **79**(1-2): 251-274.

Pan, J. (2007) Theoretical and Process Studies of the Abatement of Fuel Gas Emissions during Iron Ore Sintering (in Chinese), PhD Dissertation, Southcentral Univeristy of China.

Pang, J., Wen, X., Sun, X. (2016). Mixing ratio and carbon isotopic composition investigation of atmospheric CO_2 in Beijing, China. Sci Total Environ, **539**: 322-330.

Pataki, D. E., Bowling, D.R., Ehleringer, J.R. (2003). Seasonal cycle of carbon dioxide and its isotopic composition in an urban atmosphere: Anthropogenic and biogenic effects. Journal of Geophysical Research-Atmospheres, **108**(D23): 1-8.

Pataki, D. E., Bowling, D.R., Ehleringer, J.R., Zobitz, J.M. (2006). High resolution atmospheric monitoring of urban carbon dioxide sources. Geophysical Research Letters, **33**(3): 1-5.

Pataki, D. E., Ehleringer, J.R., Flanagan, L.B., Yakir, D., Bowling, D.R., Still, C.J., Buchmann, N., Kaplan, J.O., Berry, J.A. (2003). The application and interpretation of Keeling plots in terrestrial carbon cycle research. Global Biogeochemical Cycles, **17**(1): 1-14

Pataki, D. E., Lai, C., Keeling, C.D., Ehleringer, J.R. (2007). Insights from stable isotopes on the role of terrestrial ecosystems in the global carbon cycle. Terrestrial Ecosystems in a Changing World, Springer: 37-44.

Pataki,D.E., Emmi,P.C., Forster,C.B., Mills,J.I., Pardyjak,E.R., Peterson,T.R., Thompson,J.D., Dudley-Murphy,E., An integrated approach to improving fossil fuel emissions scenarios with urban ecosystem studies. Ecological Complexity, 2009, **6**(1): 1-14.

Peters,W., Jacobson, A.R., Sweeney, C., Andrews, A.E., Conway, T.J., Masarie, K., Miller, J.B., Bruhwiler, L.M., Petron, G., Hirsch, A.I., Worthy, D.E., van der Werf, G.R., Randerson, J.T., Wennberg, P.O., Krol, M.C., Tans, P.P. (2007) An atmospheric perspective on North American carbon dioxide exchange: CarbonTracker, Proceedings of the National Academy of Sciences, **104**(48): 18925-18930.

Prairie, Yves T., Duarte, C. M. (2007). Direct and indirect metabolic CO_2 release by humanity. Biogeosciences, **4**(2): 215-217.

Rella, C. (2011). Accurate stable carbon isotope ratio measurements with rapidly varying carbon dioxide concentrations using the Picarro $\delta^{13}C$ G2101-i gas analyzer, Picarro White Paper. Picarro Inc.

Ren, L., Wang, W., Wang, J., Liu, R. (2015). Analysis of energy consumption and carbon emission during the urbanization of Shandong Province, China. Journal of Cleaner Production, **103**: 534-541.

Röckmann1 T, S Eyer, C. van der Veen1, ME Popa, B Tuzson, G Monteil1, S Houweling, Eliza Harris, D Brunner, H Fischer, G Zazzeri, D Lowry, EG Nisbet, WA Brand, JM Necki, L Emmenegger, and J Mohn (2016). In situ observations of the isotopic composition of methane at the Cabauw tall tower site. Atmos. Chem. Phys., **16**: 10469–10487.

Rose L S, Akbari H, Taha H. Characterizing the fabric of the urban environment: a case study of Greater Houston, Texas. Lawrence Berkeley National Laboratory, 2003.

Satterthwaite D. Cities' contribution to global warming: notes on the allocation of greenhouse gas emissions. Environment and Urbanization, 2008, **20**(2): 539–549.

Shen, S., Yang, D., Xiao, W., Liu, S., Lee, X. (2014). Constraining anthropogenic CH_4 emissions in Nanjing and the Yangtze River Delta, China, using atmospheric CO_2 and CH_4 mixing ratios, Advances in Atmospheric Sciences, **31**(6): 1343-1352.

Song, T., Wang Y. (2012). Carbon dioxide fluxes from an urban area in Beijing. Atmospheric Research, **106**: 139-149.

Sun, B., Dilcher, D.L., Beerling, D.J., Zhang, C., Yan, D., Kowalski, E. (2003). Variation in Ginkgo biloba L. leaf characters across a climatic gradient in China. Proceedings of the National Academy of Sciences, **100**(12): 7141-7146.

Takahashi, H. A., Konohira, E., Hiyama, T., Minami, M., Nakamura, T., Yoshida, N. (2002). Diurnal variation of CO_2 concentration, Delta C-14 and delta C-13 in an urban forest: estimate of the anthropogenic and biogenic CO_2 contributions, Tellus B, **54**(2): 97-109.

Tans, P. (1981). $^{13}C/^{12}C$ of industrial CO^2. In SCOPE 16: Carbon Qcle Modelling (B.Bolin, ed.), John Wiley and Sons, Chichester, England, 127-129.

Thoning, K. W., Tans, P.P., Komhyr, W.D. (1989). Atmospheric carbon dioxide at Mauna Loa Observatory: 2. Analysis of the NOAA GMCC data, 1974–1985. Journal of Geophysical Research, **94**(D6): 8549-8565.

Sanam Noreen Vardag, S. N., S. Hammer, I. Levin (2016) Evaluation of 4 years of continuous $^{13}C(CO_2)$ data using a moving Keeling plot method, Biogeosciences, Biogeosciences, **13**: 4237–4251.

Wada, R., Nakayama, T., Matsumi, Y., Hiyama, T., Inoue, G., Shibata, T. (2011). Observation of carbon and oxygen isotopic compositions of CO_2 at an urban site in Nagoya using Mid-IR laser absorption spectroscopy. Atmospheric Environment, **45**(5): 1168-1174.

Wang, D. (2013) Method and Empirical Research of Urban Greenhouse Gas Measurement (in Chinese), Master's Thesis, Tianjin University.

Wang, W. , D. E. Pataki (2012). Drivers of spatial variability in urban plant and soil isotopic composition in the Los Angeles basin. Plant and Soil, **350**(1-2): 323-338.

Wen, X. F., Meng, Y., Zhang, X., Sun, X., Lee, X. (2013). Evaluating calibration strategies for isotope ratio infrared spectroscopy for atmospheric $^{13}CO_2/^{12}CO_2$ measurement. Atmospheric Measurement Techniques, **6**(1): 795-823.

Wehr, R., and S. R. Saleska (2017) The long-solved problem of the best-fit straight line: application to isotopic mixing lines, Biogeosciences, **14**: 17-29.

Widory, D. (2006). Combustibles, fuels and their combustion products: A view through carbon isotopes. Combustion Theory and Modelling, **10**(5): 831-841.

Widory, D., M. Javoy (2003). The carbon isotope composition of atmospheric CO_2 in Paris. Earth and Planetary Science Letters, **215**(1-2): 289-298.

Yakir, D., L. da SL Sternberg (2000). The use of stable isotopes to study ecosystem gas exchange. Oecologia, **123**(3): 297-311.

Yang, H.M., Wang, H.Z. , Wu, Y.B. (2011). Observation and characteristics analysis of traffic flow in Nanjing. (in Chinese), Environmental Science and Technology, **24**(2): 98-101.

Zimnoch, M., Florkowski, T., Necki, J., Neubert, R. (2004). Diurnal variability of delta C-13 and delta O-18 of atmospheric CO_2 in the urban atmosphere of Krakow, Poland, Isotopes in Environmental and Health Studies, **40**(2): 129-143.

Zobitz, J. M., Burns, S.P., Reichstein, M., Bowling, D.R. (2008). Partitioning net ecosystem carbon exchange and the carbon isotopic disequilibrium in a subalpine forest. Global Change Biology, **14**(8): 1785-1800.

Zondervan, A., H. A. Meijer (1996). Isotopic characterisation of CO_2 sources during regional pollution events using isotopic and radiocarbon analysis. Tellus B, **48**(4): 601-612.

Zhou, L., Conway, T.J., White, J.W., Mukai, H., Zhang, X., Wen, Y., Li, J. and MacClune, K., (2005). Long-term record of atmospheric CO_2 and stable isotopic ratios at Waliguan Observatory: Background features and possible drivers, 1991–2002. Global Biogeochemical Cycles, **19**(3): GB3021.

Figure 1. Dependence of the observed $\delta^{13}C$ on the H_2O mole fraction. The lines represent Equation 2. Error bars are ± one standard deviation of 1-min averages. The data in the left panel was obtained on October 1, 2014 using a 439 μmol mol^{-1} standard gas and the true $\delta^{13}C$ value of -32.8 ‰, and that in the right panel on June 10, 2015 using a 488 μmol mol^{-1} standard gas and the true $\delta^{13}C$ value of -34.1 ‰.

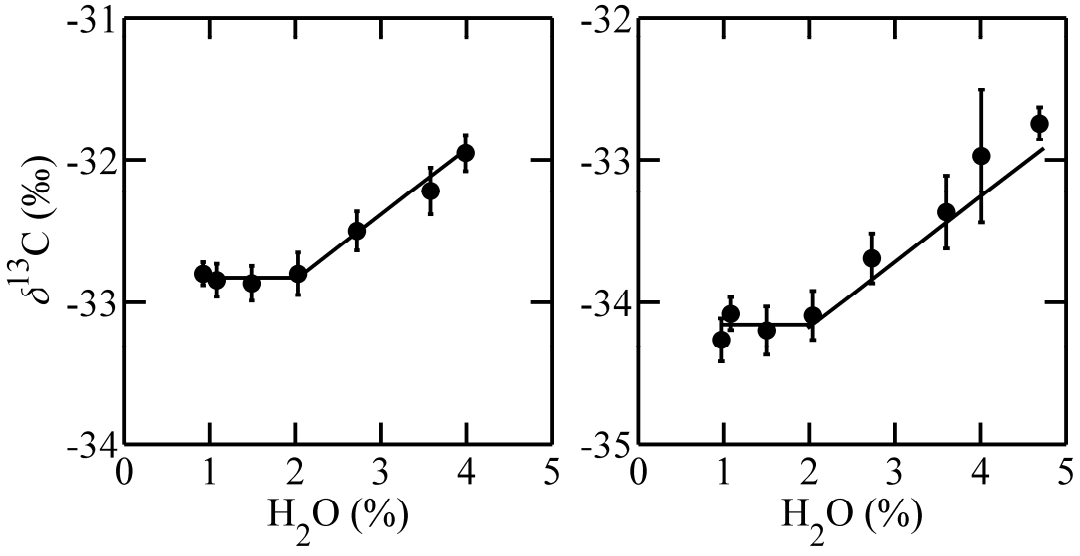

Figure 2. Monthly total CO_2 mole fraction (upper panel) and $\delta^{13}C$ (lower panel): Solid lines with circles: whole-day means; dashed lines with up triangles: daytime (10:00-16:00) means; dashed line with down triangles: nighttime (22:00-6:00) means; smooth solid lines, monthly means observed at WLG.

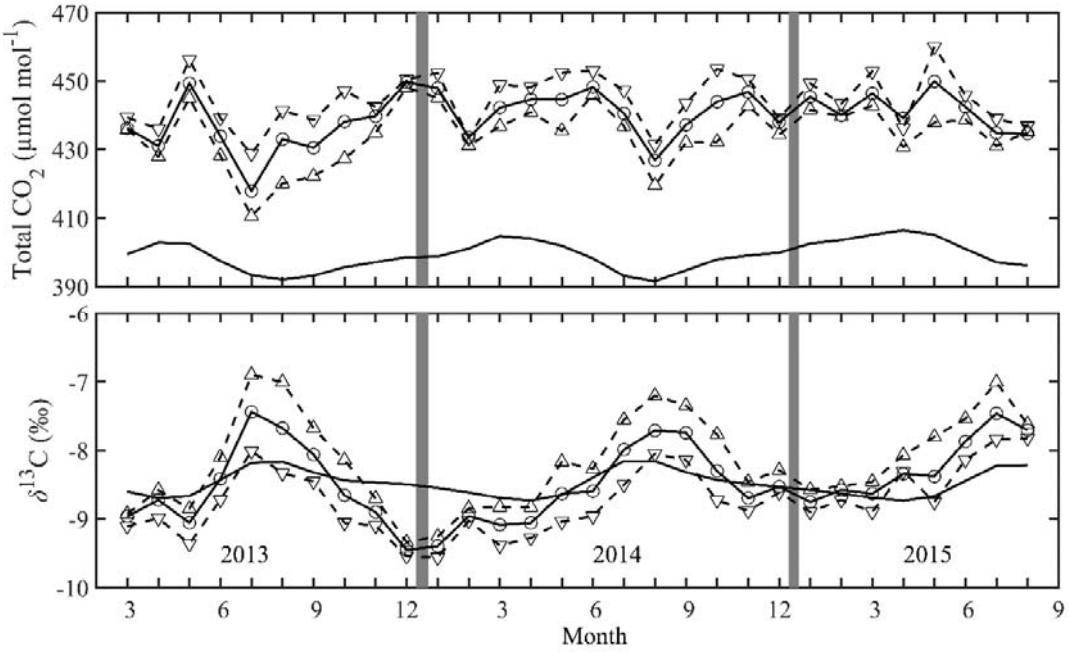

930 **Figure 3**. Mean diel variation of the CO_2 mole fraction (upper panels) and the $\delta^{13}C$ value

931 (bottom panels) between March, 2013 and August, 2015.

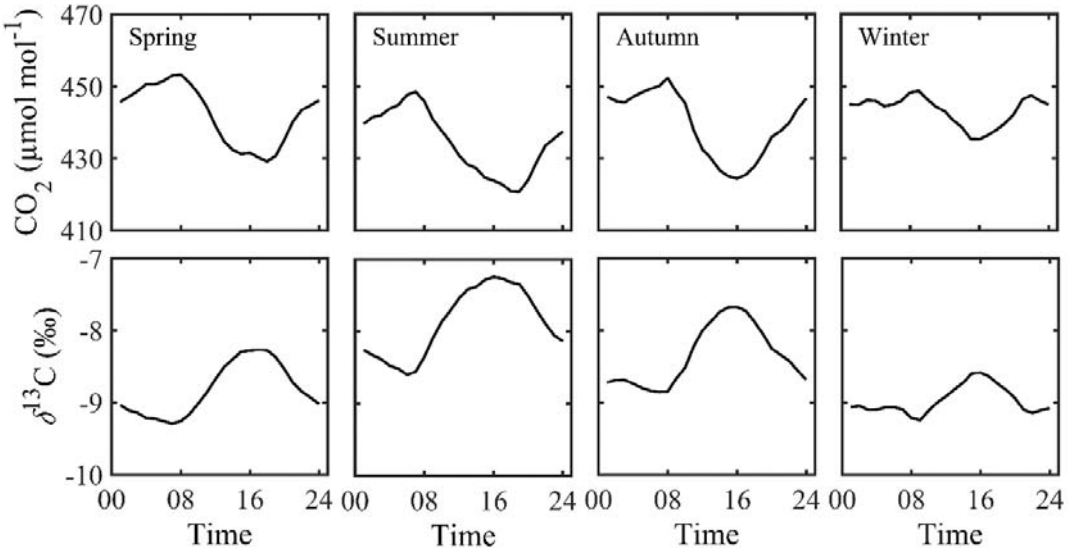

932

933

Figure 4. Application of the Miller-Tans method to the daytime (10:00-16:00) data obtained in January 2014. Each data point is one hourly mean. The solid line is the least squares regression according to Equation 3. Errors bounds on the regression coefficients are 95 % confidence intervals.

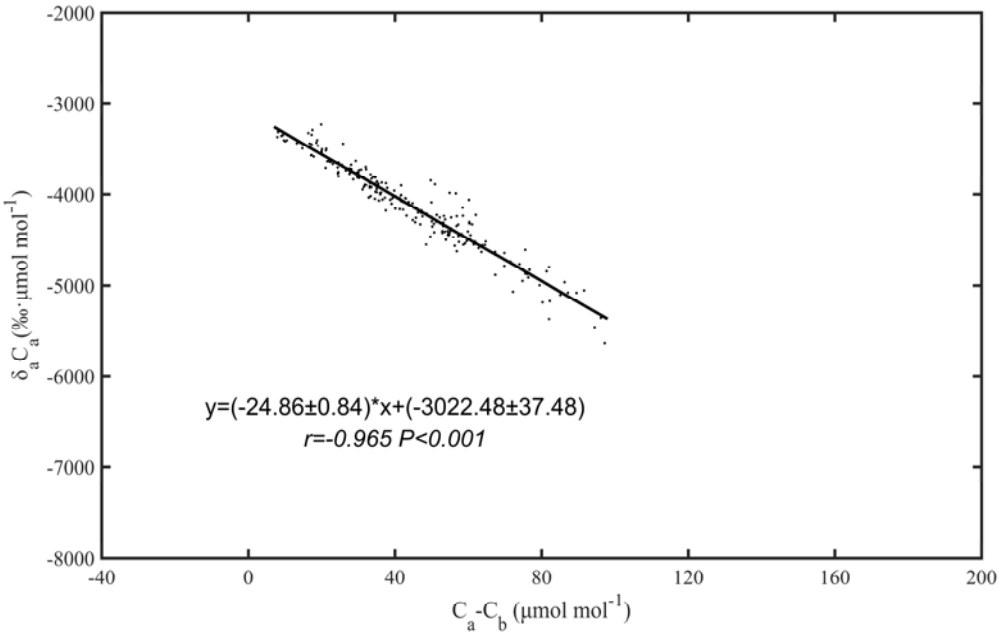

939 **Figure 5**. Same as Figure 4 but for nighttime (22:00-6:00) data obtained in January 2014.

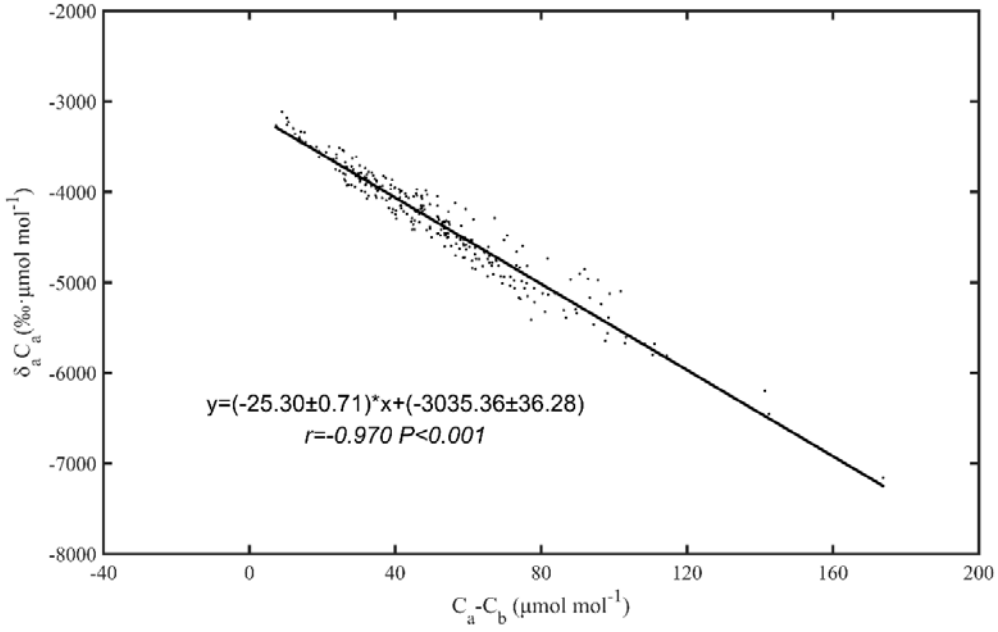

940

941 **Figure 6**. Time series of monthly $^{13}C/^{12}C$ ratio of surface sources in the YRD (a) and in

942 Nanjing (b), obtained from daytime and nighttime measurement, respectively. The error bars

943 are ± one standard deviation of the regression coefficient.

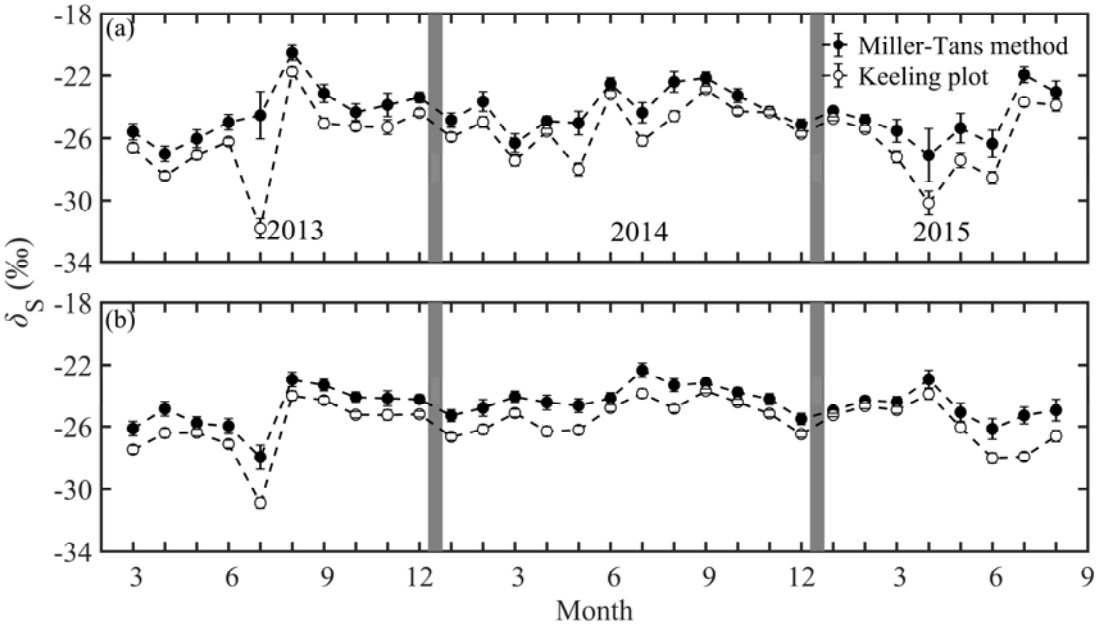

944

945

946

947

Figure 7. Time series of monthly net surface CO_2 flux (F_S), biological CO_2 flux (F_P), anthropogenic CO_2 flux excluding cement emission (F_F) and cement CO_2 flux (F_c) in the YRD. All the CO_2 mass fluxes are in mg m^{-2} s^{-1}. The flux terms F_F and F_c are assumed to have a 10 % uncertainty typical of fossil fuel consumption data. The partitioning results (F_P and F_S) are based on the source $^{13}C/^{12}C$ ratio derived from daytime atmospheric measurements.

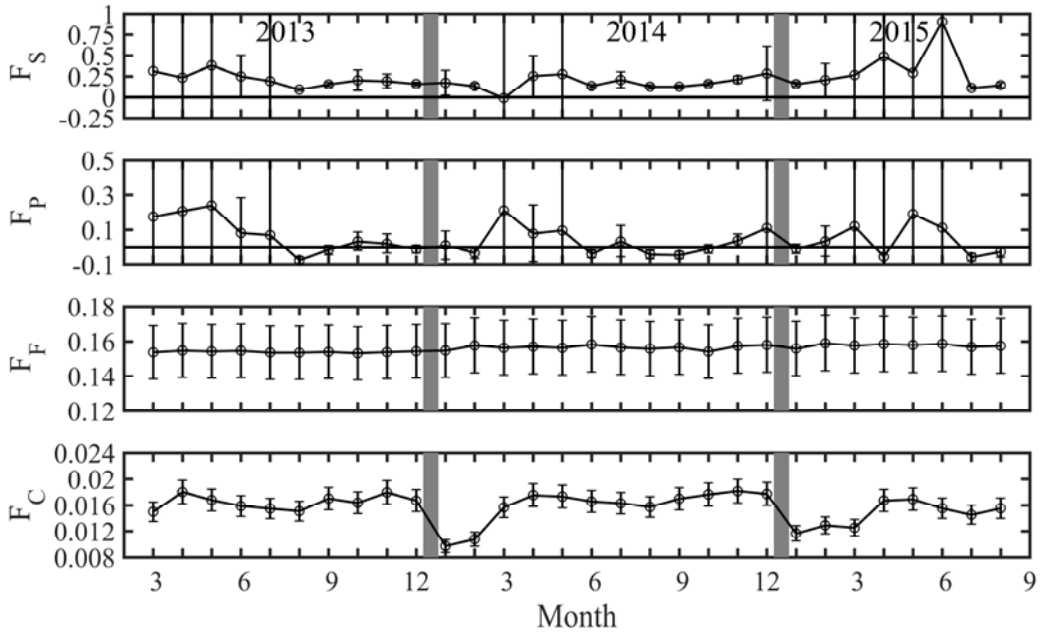

955 **Figure 8**. Time series of monthly net surface CO_2 flux (F_S), biological CO_2 flux (F_P),

956 anthropogenic CO_2 flux excluding cement emission (F_F) and cement CO_2 flux (F_c) in

957 Nanjing. All the CO_2 mass fluxes are in mg m^{-2} s^{-1}. The flux terms F_F and F_c are assumed to

958 have a 10 % uncertainty typical of fossil fuel consumption data. The partitioning results (F_P

959 and F_S) are based on the source $^{13}C/^{12}C$ ratio derived from nighttime atmospheric

960 measurements.

961

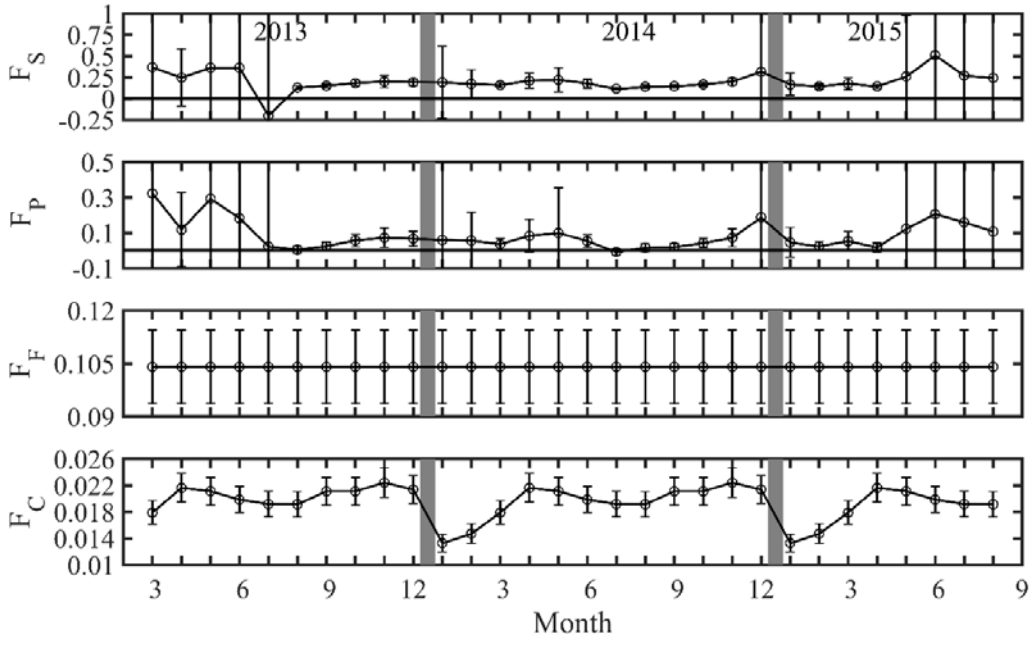

962

963 **Table 1** Standard gases used for instrument calibration. The mean and standard deviation of

964 the CO_2 mole fraction and $\delta^{13}C$ were based on 6 and 5 repeated measurements, respectively.

ID	CO_2 (μmol mol^{-1})	$\delta^{13}C$ (‰)	Period
1 Low	381.89 ± 0.99	-29.75 ± 0.27	Mar, 2013 - Aug, 2014
1 High	502.35 ± 0.28	-30.01 ± 0.18	Mar, 2013 - Aug, 2014
2 Low	380.92 ± 0.95	-29.75 ± 0.27	Sep, 2014 - Aug, 2015
2 High	501.05 ± 0.33	-30.01 ± 0.18	Sep, 2014 - Aug, 2015

965

966 **Table 2** Percentage of "fossil-plus" sources and their $\delta^{13}C$ values for the YRD and Nanjing.

967 The uncertainty in the total "fossil-plus" source is a weighted mean of the individual

968 uncertainties.

	Percentage (%)		$\delta^{13}C$ (‰)		
Sources	YRD	Nanjing	YRD	Nanjing	References
Coal	70.0	52.3	-25.46 ± 0.39	-25.46 ± 0.39	Duan, 1995, Widory 2003
Gasoline	2.1	11.4	-28.69 ± 0.50	-28.69 ± 0.50	Widory and Javoy 2003
Diesel	3.2	1.6	-28.93 ± 0.26	-28.93 ± 0.26	Widory 2006
Fuel oil	2.1	0.3	-29.32 ± 0.15	-29.32 ± 0.15	Widory and Javoy 2003
Natural gas	2.7	5.0	-39.06 ± 1.07	-39.06 ± 1.07	Widory 2003
LPG	0.7	0.2	-31.70 ± 0.40	-31.70 ± 0.40	Widory 2006
Pig iron	8.7	12.7	-24.90 ± 0.40	-24.90 ± 0.40	Pan 2007
Crude steel	1.5	0.7	-25.28 ± 0.40	-25.28 ± 0.40	Wang 2013
Ammonia synthesis	9.0	15.9	-28.18 ± 0.55	-28.18 ± 0.55	An 2012
Total	100	100	-26.36 ± 0.42	-26.97 ± 0.46	

969

Table 3. Inventory data for the isotopic composition of surface CO_2 sources and their percentage of contribution in the YRD and in Nanjing. Here the "fossil-plus" category includes all non-cement anthropogenic emissions listed in Table 2. The cement isotopic ratio is based on Andres et al. (1994). The uncertain range in the biological isotope ratio is based on Vardag et al. (2016).

Sources	YRD		Nanjing	
	$\delta^{13}C$ (‰)	Percentage (%)	$\delta^{13}C$ (‰)	Percentage (%)
"Fossil-plus"	-26.36 ± 0.42	91.0	-26.97 ± 0.46	96.4
Cement	0 ± 0.30	9.0	0 ± 0.30	3.6
Anthropogenic	-23.99 ± 0.41	100	-26.00 ± 0.45	100
Biological	-28.20 ± 1.00	——	-28.20 ± 1.00	——